Reflectance of Broken Cloud Fields: Simulation and Parameterization

FRANÇOIS-MARIE BRÉON

Laboratoire d'Optique Atmosphérique, Université des Sciences et Techniques de Lille, Villeneuve d'Ascq, France

(Manuscript received 7 February 1991, in final form 10 September 1991)

ABSTRACT

The transfer of solar irradiance in plane parallel and broken cloud fields is simulated using a Monte Carlo method. The angular distribution pattern of radiances exiting the cloud layer is studied with varying cloud geometries, optical thicknesses, cloudiness, and solar zenith angles. A rather large anisotropy of the reflected flux is found, usually increasing with solar zenith angle and with patterns that strongly depend on cloud geometry. The main features are 1) a local maximum of reflected intensity in the forward direction for all cases, 2) a limb darkening for the plane parallel case, and 3) a limb brightening and a local maximum of reflected intensity in the backward direction for broken clouds. A parameterization for the azimuth-averaged reflectance function is developed. It reproduces the Monte Carlo simulation with a reasonable accuracy and illustrates that, when azimuthally averaged, the reflectance function is dominated by side viewing and intercloud shadowing effects.

1. Introduction

Because of their large and highly variable effect on the earth and surface radiation budgets, clouds constitute one of the main climate forcings. Numerical simulations with general circulation models have shown a large sensitivity to the cloud parameters. It is therefore essential for climate change prediction to have a good understanding and modeling of cloud–radiation interactions.

Plane-parallel cloud albedo as a function of cloud liquid water content was studied by Stephens (1978), both theoretically and experimentally. This research was extended to the case of isolated finite clouds (e.g., McKee and Cox 1974; Aida 1977; Davies 1978). Further research (e.g., Weinmann and Harshvardhan 1982; Claußen 1982; Kobayashi 1989; Coakley and Kobayashi 1989) showed that the albedo of a broken cloud field was rather different than its plane parallel counterpart. Because radiation can escape through the cloud sides, the albedo is reduced at low solar zenith angles, but the enhanced intercepting surface increases the cloud field albedo at large solar zenith angles. Welch and Wielicki (1984) studied the effect of cloud shape on cloud albedo. This research leads to parameterizations of the cloud field albedo as a function of its geometry and solar zenith angle (e.g., Schmetz 1984; Welch and Wielicki 1985; Kobayashi 1988).

Although the cloud albedo is a crucial parameter in radiation budget studies, the angular distribution of reflected radiation is also needed for both observation and modeling. Derivation of reflected flux using single directional measurements requires the use of bidirectional reflectance distribution functions (BRDFs)—the ratio of the reflected radiance distribution to that of an isotropic surface reflecting the same irradiance. Such functions have been obtained empirically by averaging a large set of observations sorted by surface type, cloud type, and solar zenith angle (e.g., Ruff et al. 1968; Minnis and Harrison 1984; Taylor and Stowe 1984) and are used to correct satellite observations (Jacobwitz et al. 1984; Smith et al. 1986; Wielicki and Green 1989). Davies (1984) has used a Monte Carlo method to study the reflected radiance from broken clouds of varying optical thicknesses, aspect ratios, and solar zenith angles. He showed large departures from isotropy, maximal for nadir and limb viewing but minimal at the 60° viewing zenith angle, suggesting a preferred usage of this viewing angle for radiation budget studies.

In this context, the present study's objective is to theoretically simulate BRDFs of various cloud types in order to: 1) understand the processes that lead to anisotropic BRDFs functions, 2) recognize the cloud geometry parameters that affect most of the BRDFs, and 3) develop a parameterization for the directional reflectance of broken cloud fields as a function of the cloud field geometry and the solar angle.

In the following section we give a brief description of our Monte Carlo model. Section 3 compares its results with other results reported in the literature. Section 4 analyzes model-computed BRDFs for various cloud types and solar zenith angles. In section 5, we develop

Corresponding author address: Dr. François-M. Bréon, Laboratoire d'Optique Atmosphérique, Bat P5, USTL, 59655 Villeneuve d'Ascq Cedex, France.

a parameterization for the directional reflectance of broken cloud fields. This parameterization is discussed in section 6 and a conclusion is given in section 7.

2. The radiative transfer model

Applied to optical radiative transfer problems, the Monte Carlo method (hereafter referred to as MC) numerically simulates the path of photons interacting with a given medium. These interactions are randomly calculated according to a given optical thickness, phase function, and scattering albedo. The pathlength, λ, between two interactions within the medium is given by

$$\lambda = -\frac{1}{k_{\text{ext}}} \ln(\text{RAN}_\lambda), \quad (1)$$

where RAN_λ is a random number between 0 and 1, and k_{ext} is the volume extinction coefficient. The scattering angle, α_0, defined by the travel directions before and after one interaction, is obtained from the phase function $P(\alpha)$ of the scattering medium by

$$\int_0^{\alpha_0} P(\alpha) \sin(\alpha) d\alpha = \text{RAN}_\alpha \int_0^{\pi} P(\alpha) \sin(\alpha) d\alpha, \quad (2)$$

where RAN_α is another random number between 0 and 1. The other angle required to define the new travel direction after an interaction, the rotation around the propagation direction, is randomly chosen between 0 and 2π.

The single-scattering albedo, ω_0, defines the probability for a photon to be scattered, rather than absorbed, during an interaction with a cloud droplet ($\omega_0 = 1$: no absorption; $\omega_0 = 0$: no scattering). Absorption by the medium can be modeled either by randomly deciding at each interaction if the photon is absorbed by the medium, or, as in the case of the more efficient method used in this study, by giving the photon a weight W equal to

$$W = (\omega_0)^{N_{\text{inter}}}, \quad (3)$$

where N_{inter} is the number of interactions the photon undergoes within the medium.

In our model, broken cloud shapes are approximated by cylinders. Even though broken cloud geometry is far more complex than simple cylinders, this modeled arrangement probably represents the real world better than cubes—the geometry used in most other reported Monte Carlo simulations. Bradley (1981), for instance, reported a large number of almost perfect cylinders when observing growing cumulus. The cubic cloud geometry was also used in the present study for comparison purposes. In the case of infinite plane parallel clouds, the optical thickness is the only macroscopic parameter needed to define the cloud. In the case of the broken cloudiness, the optical thickness in both vertical and horizontal dimensions and the mean cloudiness are parameters that can vary. The simulated *clouds* are distributed on a regular square array.

The model clouds are illuminated through the top and sides from a given direction defined by the solar zenith angle θ_s. These clouds are to be homogeneous and embedded in a nondispersing atmosphere, meaning that Rayleigh scattering and absorption by the atmosphere are neglected. Surface reflectance is also neglected. Cloud–cloud interactions, however, are taken into account; i.e., a photon exiting one side of a cloud can reenter another. Similarly, mutual shadowing effects at large solar zenith angles are considered.

The cloud optical thickness is equal to the volume extinction coefficient multiplied by the geometrical thickness

$$\tau = k_{\text{ext}} H. \quad (4)$$

For a given cloud droplet size distribution, there is a linear relationship between cloud optical depth and liquid water content. An optical depth of 100 was the usual limit for our computations, which corresponds to a precipitable liquid water content of about 0.39 mm.

Deirmendjian (1969) computed and reported a series of phase functions for various wavelengths and cloud types. For our study we chose the cumulus type droplet distribution ($C1$) at a wavelength of 0.45 μm, giving an optical depth of 1 for a liquid water content of 3.86 g m^{-2}. The Deirmendjian phase function shows a very strong forward peak and two weaker backward peaks—one strictly in the backward direction and another at 35°. For this particular water droplet distribution, 96% of the photons are scattered in the forward hemisphere, of which 50% are in the first 8°.

Another phase function, the Henyey–Greenstein function, is often used for MC studies applied to solar radiation transmission within clouds. This particular function, with an asymmetry factor g of 0.85, is a simpler analytical approximation of the phase functions that can be computed using Mie theory. It was also used in our study for comparison purposes.

3. Comparison with other Monte Carlo models

Many other MC simulation results have been reported in the literature, and we first tried to reproduce them for validation purposes. The comparison of our model results with others (e.g., Davies 1978, 1984; Crétel et al. 1989) has shown an agreement within the statistical uncertainty inherent to MC computations, which gave us confidence in the validity of our computations. We also found differences with other reported results. The cases for which significant differences were found are reported below.

Figure 1 compares the cloud reflectance of a plane parallel cloud as a function of optical thickness for solar zenith angles of 0° and 60° as found by our model and those reported in McKee and Cox (1974) and Davies (1978). Davies only reported results for an optical thickness of 73.5.

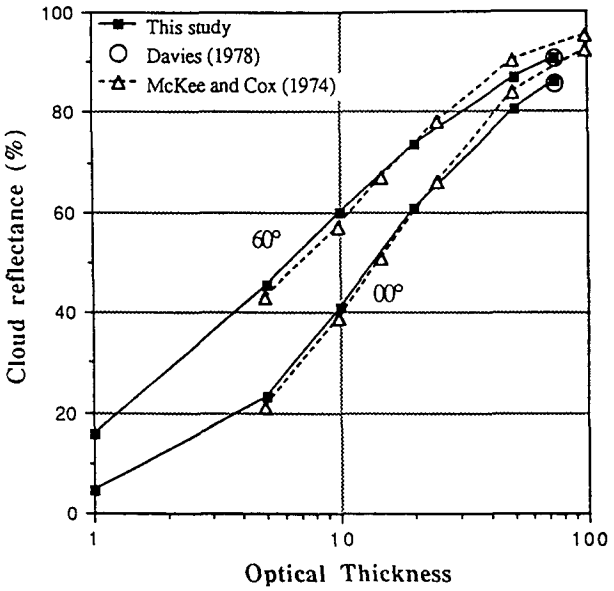

FIG. 1. Reflectance of a plane parallel cloud as a function of its optical thickness, as found by three Monte Carlo methods: the present study (squares), the McKee and Cox model (triangles), and the Davies model (circles). Results are given for solar zenith angles of 0° and 60°.

As expected, the general shapes of the two curves are similar. The cloud reflectance is close to zero for very thin clouds and tends to 1 for optically thick ones. For small optical thicknesses, there is very good agreement between our model and McKee's. For large optical thicknesses, however, we find values lower than those reported in McKee and Cox (1974). Davies (1978) did report such differences and expressed confidence in his model after comparisons with other methods. As can be seen, our results agree well with Davies' for the large optical thickness he reported.

Similarly, McKee and Cox (1974) presented some results with an isolated cubical cloud using the same phase function as ours. Those results were later confirmed by Davies (1978). Comparisons with our results are presented in Table 1.

The differences found with McKee and Cox (1974) results for the lower optical thickness at 30° and 60° cannot be explained by statistical errors. For the other reported cases, differences, if any, can be explained by statistical imprecision and rounding errors. The excellent accord with the Davies results and with the majority of the McKee and Cox values gives us confidence in our model. The two cases with significant differences are not explained.

Welch and Wielicki (1984) reported results obtained with an MC model that are of particular interest for our validations because 1) they employ an array of cylinders, a geometry we want to study, and 2) they give more detailed results showing some angular dependance of the reflected flux (their Fig. 10). Figure 2 shows the results obtained with our MC model using the same geometry and scattering parameters as theirs (cloudiness = 0.7, $\omega_0 = 0.999$, $\tau = 49$, and Henyey–Greenstein phase function with $g = 0.85$). The boxes on the left of each figure give the percentage of radiation escaping through the top, bottom, and the four quarters of the cloud sides. The angular pattern depicts the angular distribution of radiation exiting the cloud sides. For a given geometry, the "first exit" considers the photons after they have gone through only one cloud (no cloud–cloud interactions), whereas the "last exit" considers the photons after their last interaction with a cloud. For each angular quadrant and position box, the scattered radiance percentage as found with our model is given, and the one reported in Welch and Wielicki (1984) is in parenthesis. The comparison shows large differences. Although none of the cases displays perfect agreement, the largest and more consequential discrepancy is found for the angular distribution of radiation out of the cloud side for the "cylinder's last exit" case. We found a distribution analogous to the cube geometry, whereas Welch and Wielicki reported large differences that were traced to the size and shape of "holes" between clouds.

Welch and Wielicki's simulations were performed with 5000 *photons;* ours with 100 000. If D is the scattered radiance percentage in one of the bins, the expected difference between the two simulations is then on the order of $\sqrt{D}/700$ (binomial distribution). Clearly, this statistical uncertainty cannot explain the differences of the "cylinder's last exit" case (D values as different as 1.7 and 8.0).

The large differences were further investigated with the help of a third, independent MC model (Crétel et al. 1989). Products similar to Welch and Wielicki's were computed and very close agreement with our model was found (Crétel and Herman 1990, personal communication). This agreement is of course not proof that our model is correct and that Welch and Wielicki's is not, since the same error could be present in Crétel's and our model's computations. It should be pointed out, however, that the two models were designed independently, which gives us confidence in our model and supports the conclusion that cubic and cylindric geometries lead to similar angular distribution patterns.

TABLE 1. Cloud reflectance for an isolated cubic cloud as found by our model, McKee and Cox (1974), and Davies (1978).

Angle (deg)	Optical thickness	McKee and Cox	Davies	This study
0	4.9	0.17		0.175
0	73.5	0.69	0.696	0.697
30	4.9	0.13		0.152
30	73.5	0.58		0.592
60	4.9	0.19		0.214
60	73.5	0.56	0.565	0.564

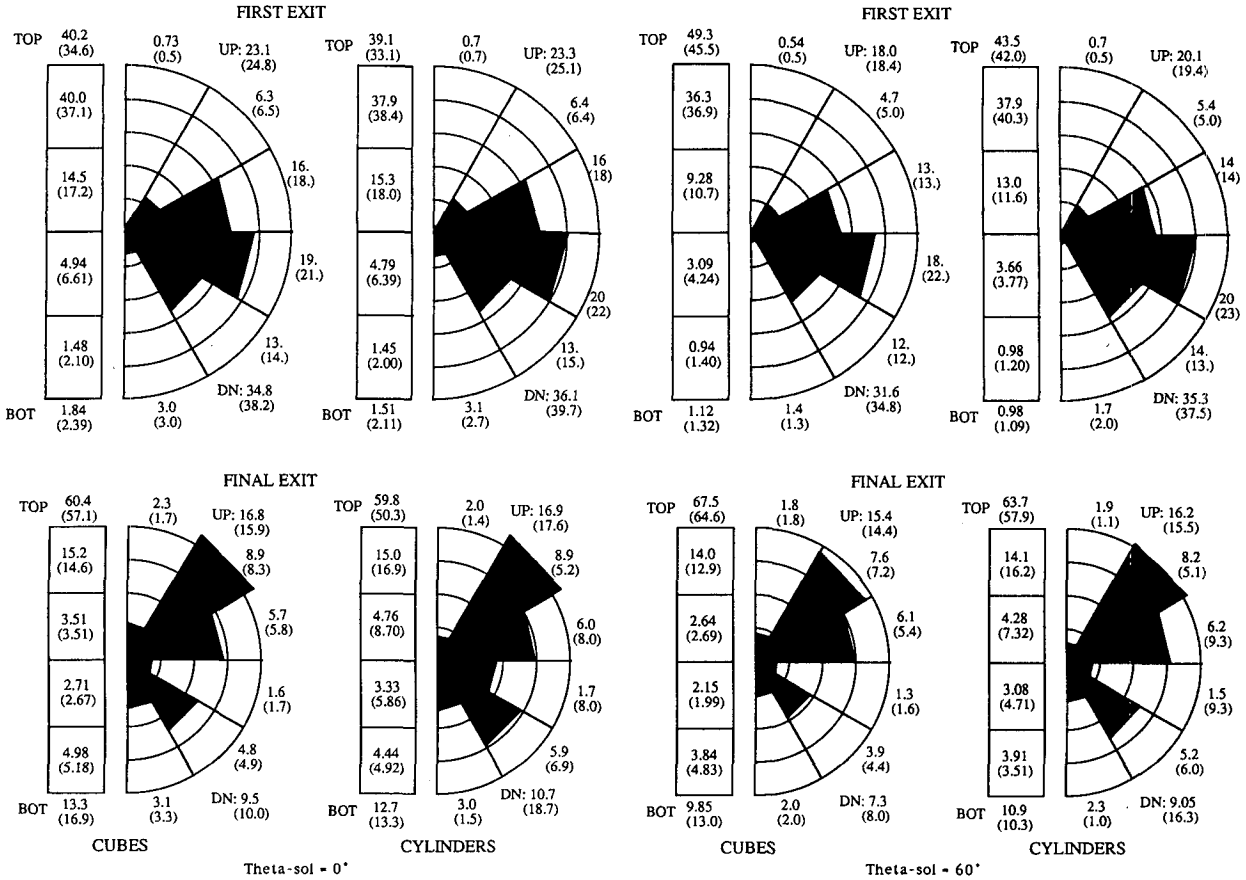

FIG. 2. Angular distribution of photons exiting cloud sides and vertical distribution of photons exiting the cylinder clouds at the first exit (top) and the final exit (bottom). The boxes to the left show the percentage of incident energy that exits each quarter of the cloud sides. The angular pattern depicts the angular distribution (six 30° increments) out of the sides with concentric circles representing 5%, 10%, 15%, 20%, and 25% (first exit) or 2%, 4%, 6%, and 8% (final exit) of incident energy: The four left-hand diagrams are for 0° solar angle; the others for 60°. Values in parentheses represent Welch and Wielicki (1984) results in their Fig. 10.

This conclusion has interesting implications for Monte Carlo simulations. From these two cases, the cubic and cylindric geometries, it seems that the cloud shape is a second-order parameter when investigating cloud field albedos and reflectance. The parameter of importance would be the cloud-intercepting surface (top and sides) rather than the cloud shape.

4. Bidirectional reflectance functions

a. Stratiform cloud fields

The stratiform cloud field is the simplest geometry as neither side effects nor cloud–cloud interactions must be considered. Once the scattering parameters (P, ω_0, k_{ext}) are chosen, the only varying parameters are the cloud optical thickness and the solar zenith angle.

Figure 3 presents a typical BRDF function for a plane parallel cloud. For nonzenith solar angles, a plane parallel cloud BRDF presents a maximum in the forward direction (Fig. 3). The forward peak of the phase function has a narrow angular width, but multiple interactions broaden the solid angle through which radiation is primarily scattered and lead to a radiation maximum in the forward direction. This maximum is rather small at solar zenith angles lower than 45° but clearly appears for solar zenith angles of 50° and larger. Figure 3 illustrates that, for a solar zenith angle of 60°, the forward peak affects viewing angles between 45° and the limb and is responsible for reflected flux intensities at the limb up to 2.5 times greater than would be obtained if the scattering were isotropic. It is clear that, as the solar zenith angle increases, this effect would affect viewing angles closer to the zenith.

The other characteristics of plane parallel cloud BRDFs is a general decrease toward the limb viewing. This decrease can be seen in Fig. 3 but is more evident when looking at azimuth-averaged reflectance functions (Figs. 4 and 5). Figure 4 shows how the reflectance function of a plane parallel cloud ($\tau = 20$) varies with the solar zenith angle. For a sun at the zenith,

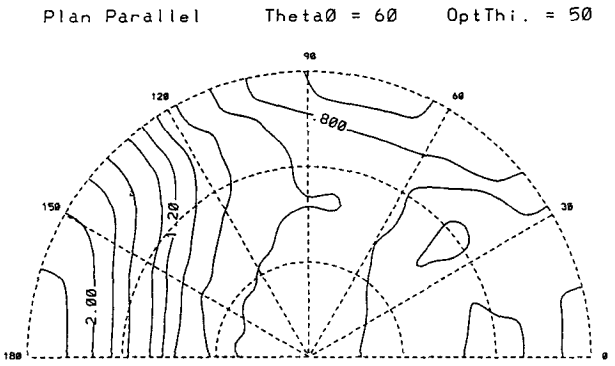

FIG. 3. Bidirectional reflectance function for a plane parallel cloud with an optical thickness of 50 and a solar zenith angle of 60°. The sun is on the right side of the chart. The radius is a linear function of the viewing zenith angle (from 0° to 90°), and the polar angle is the viewing azimuth angle (the sun direction is at 0°). The contour interval is 0.1 when the values are smaller than 1.3. For larger values, the contour lines are 1.3, 1.5, 1.7, 2., 2.5, 3, ...

there cannot be any forward maximum and the only feature is the limb darkening. This effect is explained by the fact that a photon moving in a near-horizontal direction has a smaller chance of exiting the cloud before going through another interaction that may redirect it than has a photon moving at an angle closer to the vertical, which takes a shorter path. As the solar zenith angle increases, the forward maximum is increasingly present at large viewing angles. Note that for a sun at the zenith, the limb darkening reduces the BRDF to about 0.5. The optical thickness effect on plane parallel cloud BRDFs is presented in Fig. 5 for

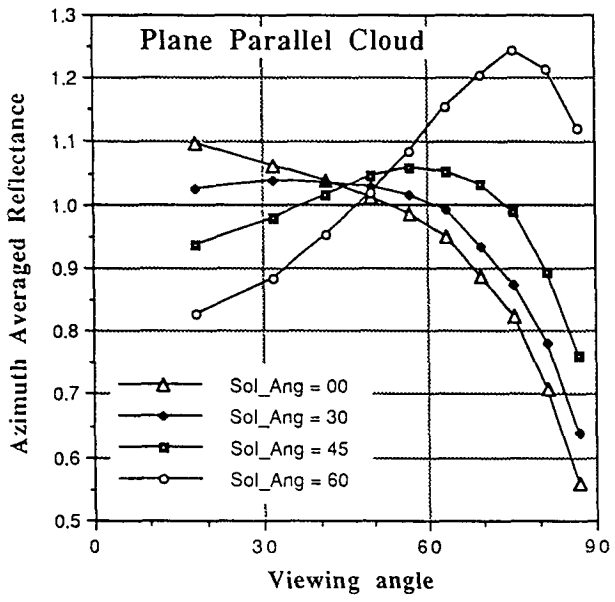

FIG. 4. Azimuth-averaged reflectance function for a plane parallel cloud of optical thickness 20 at varying solar zenith angles.

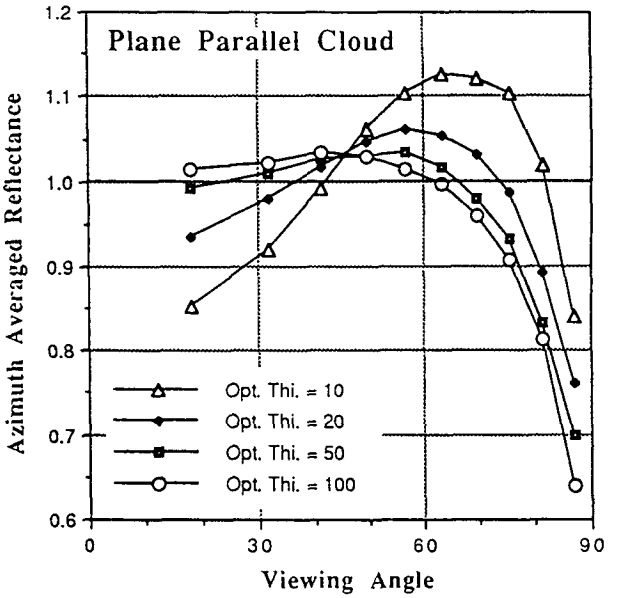

FIG. 5. Azimuth-averaged reflectance function for plane parallel cloud of varying optical thicknesses. The solar zenith angle is 45°.

a solar zenith angle of 45°. For rather thin clouds ($\tau = 10$), the photons that have gone through few scattering interactions dominate the reflected flux and we clearly see the forward maximum effect at large viewing angles. As the cloud optical thickness increases, more photons exit the cloud top after many interactions. These photons have lost the "memory" of their initial direction and only show the limb-darkening effect, smoothing in the forward maximum.

b. *Single cloud*

An isolated cloud is the limit of a broken cloud field toward low cloudiness. It is a simpler case since neither cloud–cloud interaction nor shadowing of incoming radiation is involved. For such a cloud *field,* the BRDF shows a strong general increase with increasing zenith viewing angle (Fig. 6). This feature can be understood considering that each face of the cloud approximately emits isotropically. If so, and for a cylinder-shaped cloud, the radiance $R(\theta_v, \phi)$ scattered by the medium in a direction of zenith angle θ_v would be equal to

$$R(\theta_v, \varphi) = F_{\text{top}} \frac{\cos\theta_v}{\pi} + \frac{2}{\pi} F_{\text{side-up}} \frac{\sin\theta_v}{\pi}, \quad (5)$$

where F_{top} and $F_{\text{side-up}}$ are the fluxes exiting the top and sides, respectively, in the upward direction. This value is normalized (divided) by $(F_{\text{top}} + F_{\text{side-up}}) \cos\theta_v/\pi$, which is the radiance scattered by an isotropic horizontal surface that reflects the same flux. With this approximation, the BRDF is therefore expected to be

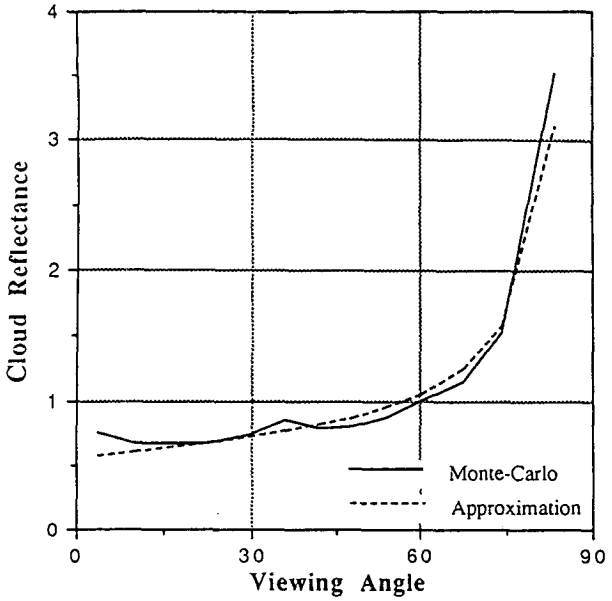

FIG. 6. Reflectance as a function of viewing zenith angle for an isolated cylindrical cloud ($\tau = 30$) with the sun at zenith. The dotted curve gives the MC model results; the solid line is the approximation where each face scatters the radiation isotropically (see text). For this particular solar angle, all azimuth directions are equivalent.

$$\mathrm{BRDF}(\theta_v, \varphi) = \frac{F_{\text{top}}}{F_{\text{top}} + F_{\text{side-up}}} + \frac{2}{\pi}\frac{F_{\text{side-up}}}{F_{\text{top}} + F_{\text{side-up}}}\tan(\theta_v). \quad (6)$$

We used our MC method for an isolated cylindrical cloud of optical thickness 30 and illuminated by the sun at the zenith; $F_{\text{top}} = 29\%$ and $F_{\text{side-up}} = 23\%$ of the intercepted incoming flux. Following our hypothesis of isotropic scattering by each side, the reflectance function is expected to be equal to

$$\mathrm{BRDF}(\theta_v, \varphi) = 0.55 + 0.29\tan(\theta_v). \quad (7)$$

Figure 6 shows the results obtained with this approximation and the MC method. Both are rather similar and show that, as stated in our hypothesis, the general reflectance function shape can be modeled as if each cloud face scattered radiation isotropically. Some differences are found, however: MC model results are larger than those given by the "isotropic" theory at the zenith and limb viewing angles. These small differences are consistent with the results obtained with a thick plane parallel cloud. The flux scattered by one cloud face is larger in the orthogonal direction compared to a pure isotropic scatter (limb darkening effect). For viewing angles close to the zenith, radiance coming from the cloud sides is negligible, while the radiance coming from the top is larger than from a pure isotropic face. Similarly, at the limb, radiance coming from the top of the cloud is negligible, while the radiance coming from the side is larger than what a pure isotropic face would produce. Note also the MC result local maximum at 35°. Since the phase function presents two local maxima at 0° and 35° in the backward direction, the first-order scattering results in two radiance maxima in these directions. The MC simulation radiance maxima at 0° and 35° zenith angle result, therefore, from first-order scattering in the direction of the phase function local maxima. We repeated this study with other optical thicknesses (10, 20, and 50) and found similar agreement between the pure MC computations and the assumption of isotropic scattering through the faces, the agreement increasing with cloud optical thickness. The effect of a thick cylindrical cloud on solar radiation can therefore be modeled, in a first approximation, as if each face scattered energy as a thick plane parallel cloud does. This parameterization for nonisolated clouds will be developed in section 5.

The general increase toward the limb as presented above is modified by the phase function effect and the fact that all cloud faces are not lit the same way. Figure 7 presents the results obtained with an isolated cylindrical cloud of aspect ratio (diameter/height) equal to 1, optical thickness 50, and receiving the solar radiation at a zenith angle of 60°.

We now depict two maxima, one in the backward direction and a smaller one in the forward direction, similar to what was found with the plane parallel case. The backward maximum is increasingly present with increasing optical thickness and can get larger than the forward maximum, as is the case in Fig. 7. For large enough optical thicknesses, a small amount of incoming radiation goes from one side of the cloud to the other. Since most of the photons exit the cloud through the same face they enter, more photons escape through the cloud face into the sun than through the others, which explains the BRDF's maximum in the backward direction.

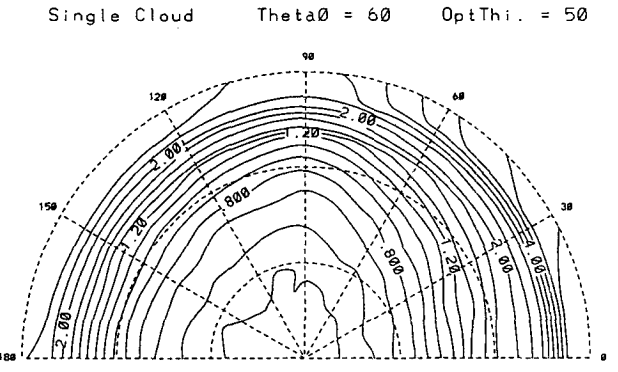

FIG. 7. Bidirectional reflectance function for a cylindric isolated *cloud* with an optical thickness of 50 and a solar zenith angle of 60°. The cylinder has an aspect ratio of 1 (diameter equal to height). Conventions and contour intervals are the same as in Fig. 3.

c. Broken cloud fields

A broken cloud field is approximately an intermediate case between the plane parallel cloud and the single cloud. Added to the effects depicted for other configurations are cloud–cloud interactions. Consequently, the BRDF tends to match the single cloud extreme when the distance between clouds increases. For smaller distances, interactions between clouds modify the BRDF, closing to the plane parallel limit as the holes between the clouds fill up.

Figures 8a and 8b are two examples of the many BRDFs found while varying the cloud aspect ratio, cloudiness, optical thickness, and solar zenith angle. Each cloud has the same geometry as in Fig. 7 (single cloud/low cloudiness limit), but the mean cloudiness has been set to 0.10 (Fig. 8a) and 0.5 (Fig. 8b). One can thus follow the BRDF's evolution as the cloudiness increases with the Figs. 7, 8a, 8b, and 3 (plane parallel limit). Even a low cloudiness (10%) greatly reduces the BRDF unlimited increase toward the limb. For smaller viewing zenith angles, cloud–cloud interaction effects are much weaker and the cloud field BRDF is close to its single cloud counterpart. For increased cloudiness (50%), the general BRDF increase toward the limb is still present, but the maximum in the forward direction, as in the plane parallel case, now dominates.

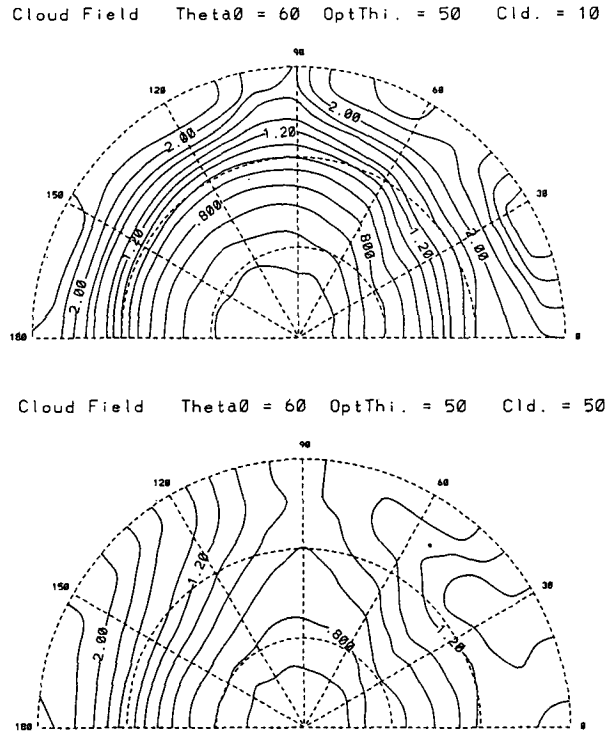

FIG. 8. Bidirectional reflectance function for an array of cylindrical *cloud* (τ = 50) with a solar zenith angle of 60°. Each cylinder is similar to the one used for Fig. 9. Nebulosity is equal to 0.10 (Fig. 10a) and 0.5 (Fig. 10b). Conventions and contour intervals are the same as in Fig. 3.

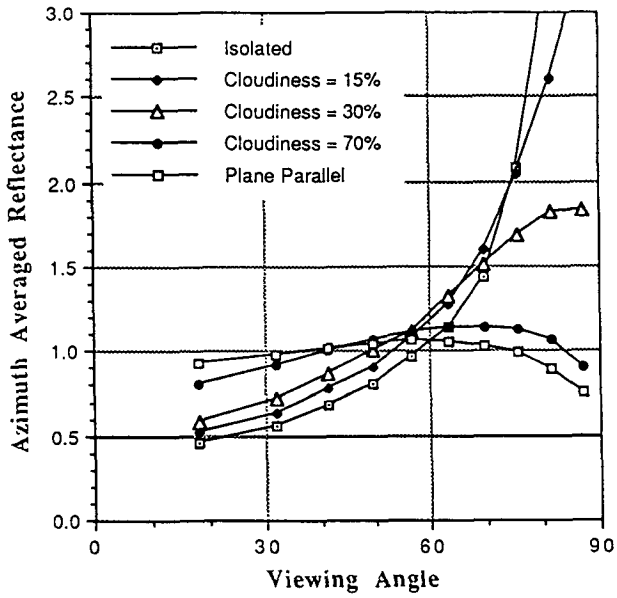

FIG. 9. Azimuth-averaged reflectance function for regular arrays of cylindrical *clouds* at varying cloudiness. Each cloud has an optical thickness of 20 and aspect ratio of 1. The solar zenith angle is 45°.

The azimuth-averaged results (Fig. 9) clearly show the rapid BRDF weakening at large viewing zenith angles as the cloudiness increases. As the neighboring clouds close up, a larger part of the photons escaping a cloud side with a large zenith angle is intercepted before it can escape to space. Eventually, when the geometry reaches the plane parallel limit, photons can only escape the cloud top, and the side-viewing effect disappears. On the other hand, the BRDF maximum away from the sun is rather insensitive to the cloudiness changes because most photons leaving the medium in that direction escape the cloud through the top.

The main features depicted in the BRDF of a broken cloud field are 1) an increase of the outgoing radiance toward the limb, 2) a maximum in the forward direction owing to the phase function effect, and 3) a maximum in the backward direction owing to the incoming flux's spatial distribution on the cloud sides. As the cloudiness increases, the second feature grows in importance while the third weakens.

5. Parameterization

Our objective is to develop a parameterization for the broken cloud field reflectance as a function of cloudiness, optical thickness, aspect ratio, and solar zenith angle. Although an ultimate goal is to have a parameterization for BRDFs, we decided, as a simpler initial step, to work on azimuth-averaged results. Clearly, such parameterization cannot be used for sat-

ellite measurements normalization since the BRDF azimuth variations are as large as the variations with zenith angle. It could be used, however, for measurement extrapolation to zenith angles not accessible to polar satellite instruments. Moreover, when computing atmospheric absorption of reflected irradiance, a parameter of importance is the radiance distribution with respect to the zenith angle, independent of azimuth angle. The parameterization could then be used for a simple description of reflected radiance angular distribution.

Our parameterization is based on the observation that, for reasonably thick clouds, the reflectance function of broken cloud fields is dominated by side-viewing effects and intercloud shadowing. We therefore seek a modeling of these effects only, assuming that the cloud faces radiate isotropically. This hypothesis will then be verified by comparing MC simulations to the parameterization.

Let R be the cloud radius, H the cloud height, and D the mean distance between a cloud and its neighbors. The cloud aspect ratio K is equal to $2R/H$ and, for a regular array of cylinders, the ratio D/H should depend on the cloudiness "cld" only.

The incoming flux intercepted by a cloud top is

$$FT_0 = F_0 \pi R^2 \cos(\theta_s), \tag{8}$$

where F_0 is the incoming radiance and θ_s the solar zenith angle.

When no shadowing occurs, the incoming flux intercepted by the cloud side is

$$FS_0 = F_0 2RH \sin(\theta_s) = F_0 \frac{4R^2}{K} \sin(\theta_s). \tag{9}$$

We neglect the intermediate case of cylinder mutual shadowing [see Welch and Wielicki (1984) for details]. For large solar zenith angles, because of cloud mutual shadowing, the incoming flux intercepted by the cloud side reduces to

$$FS_0 = F_0 R^2 \left(2 \left(\frac{\pi}{\text{cld}} \right)^{1/2} - \pi \right) \cos(\theta_s). \tag{10}$$

We are interested solely in the mutual contribution of the top and sides. The flux intercepted by the top to 1 ($FT_0 = 1$) can therefore be normalized and

$$FS_0 = \min \left[\frac{4}{K\pi} \tan(\theta_s), \left(\frac{4}{\pi \times \text{cld}} \right)^{1/2} - 1 \right] \tag{11}$$

can be obtained.

We now study an isolated cloud to seek the flux exchanges between the sides and top. Let us take A_{tt}, A_{ts}, and A_{tb} as the flux ratios that, after entering through the top, exit through the top, side, and bottom, respectively. Similarly, A_{st}, A_{ss}, and A_{sb} are the flux ratios that, after entering the cloud through the side, exit through the top, side, and bottom, respectively. Then

$$A_{tt} + A_{ts} + A_{tb} = 1 \tag{12a}$$

$$A_{st} + A_{ss} + A_{sb} = 1 \tag{12b}$$

$$A_{st} = A_{sb}. \tag{12c}$$

Each of these coefficients depend on the cloud optical thickness and its aspect ratio. We neglect their dependence on the spatial and angular distribution of incoming radiance and therefore on the solar zenith angle and the cloud field geometry. We used our Monte Carlo model for different geometries and fitted the results to simple analytical expressions:

$$A_{tt} = 1 - \exp(-C\tau K^a), \tag{13a}$$

with $C = 0.892\ 10^{-2}$ and $a = 0.6293$:

$$A_{ts} = \exp\left[-K \left(b\tau + \frac{c}{\tau} \right) \right], \tag{13b}$$

with $b = 0.6005\ 10^{-2}$, $c = 2.818$:

$$A_{ss} = L(\tau) + \frac{1 - L(\tau)}{1 + K^d} \tag{13c}$$

and with $d = 1.58$ and $L(\tau) = -0.11 + 0.17 \ln(\tau)$.

The other coefficients A_{xx} can be determined using these expressions and Eqs. (12a–c) and (13a–c). Although the above expressions do not always give coherent values at the limit, they fit the MC simulations for optical thicknesses between 10 and 100 and aspect ratios between 0.2 and 5.

The fluxes exiting the cloud side and top are

$$F_{\text{side}} = \frac{A_{ts} FT_0 + A_{ss} FS_0}{1 - \beta A_{ss}} \tag{14a}$$

$$F_{\text{top}} = A_{tt} FT_0 + A_{st} FS_0 + A_{st} \beta F_{\text{side}}, \tag{14b}$$

where β is the ratio of the flux that, after leaving a cloud side, is intercepted by a nearby cloud. The term $(1 - \beta A_{ss})$ was introduced to account for cloud–cloud interactions.

The flux exiting the cloud through the side is given by Eq. (14a), but only a fraction $(1 - \beta)$ leaves the cloud layer and subsequently participates in the cloud field reflectance. On the other hand, the total flux exiting the cloud through the top leaves the cloud layer. We subsequently obtain the relative contribution of the side and top to the flux that leaves the cloud layer

$$F_{\text{top-eff}} = \frac{F_{\text{top}}}{F_{\text{top}} + (1 - \beta) F_{\text{side}}} \tag{15a}$$

$$F_{\text{side-eff}} = \frac{(1 - \beta) F_{\text{side}}}{F_{\text{top}} + (1 - \beta) F_{\text{side}}}. \tag{15b}$$

Assuming that the flux escaping the cloud side is equally distributed over the cloud height, we seek the ratio of the radiance that, after leaving the cloud side with the zenith angle θ_v, is intercepted by a nearby

cloud. If $\tan(\theta_v)$ is less than D/H, this ratio is 0. If not, it is equal to $1 - D/[V\tan(\theta_v)]$.

Integrating over the angle θ_v, the ratio of the flux, which after leaving the cloud side is intercepted by a nearby cloud, is obtained. We find:

$$\beta = 1 - \frac{1}{\pi}\left(2\theta_0 - \sin(2\theta_0) - 2\frac{D}{H}\frac{1}{1+\left(\frac{D}{H}\right)^2}\right), \quad (16)$$

where

$$\theta_0 = \tan^{-1}\left(\frac{D}{H}\right). \quad (17)$$

Assuming that radiation exiting each cloud face is isotropic, the reflectance functions for the cloud top and the cloud sides is obtained:

$$R_{\text{top}}(\theta_v) = 1 \quad (18)$$

$$R_{\text{side}}(\theta_v) = \frac{2}{\pi(1-\beta)}\tan(\theta_v), \quad \text{if } \theta_v < \theta_0 \quad (19a)$$

$$R_{\text{side}}(\theta_v) = \frac{D}{H}\frac{2}{\pi(1-\beta)}, \quad \text{if } \theta_v > \theta_0. \quad (19b)$$

The cloud field reflectance is then given by

$$R(\theta_s) = F_{\text{top-eff}}R_{\text{top}}(\theta_s) + F_{\text{side-eff}}R_{\text{side}}(\theta_s). \quad (20)$$

Equations (11)–(20) give the azimuth-averaged reflectance as a function of optical thickness, cloud aspect ratio, solar zenith angle, mean intercloud distance, and cloudiness. As stated before, the ratio D/H should be a function of the cloudiness only. Fitting MC simulations of broken cloudiness to the formation developed above, it was found that

$$\frac{D}{H} = 2.3\left(\frac{1}{\text{cld}} - 1\right). \quad (21)$$

Note that the coefficients A_{xx} [Eq. (13)] were determined from isolated cloud simulations and that, therefore, Eq. (21) is the only one that has been fitted to MC simulations of a broken cloud field.

6. Discussion

When compared to MC simulations, the parameterization described above reproduces well the main reflectance variations with the viewing angle. Figures 10a,b compare typical MC results with the parameterization. The agreement is not perfect: The parameterization underestimates the reflectance for the low cloudiness–large viewing angle case. Similarly, the parameterization does not show the reflectance decrease at the largest viewing angles for the high cloudiness case. However, the mean shape of the curve depicting the reflectance as a function of the viewing angle is correct.

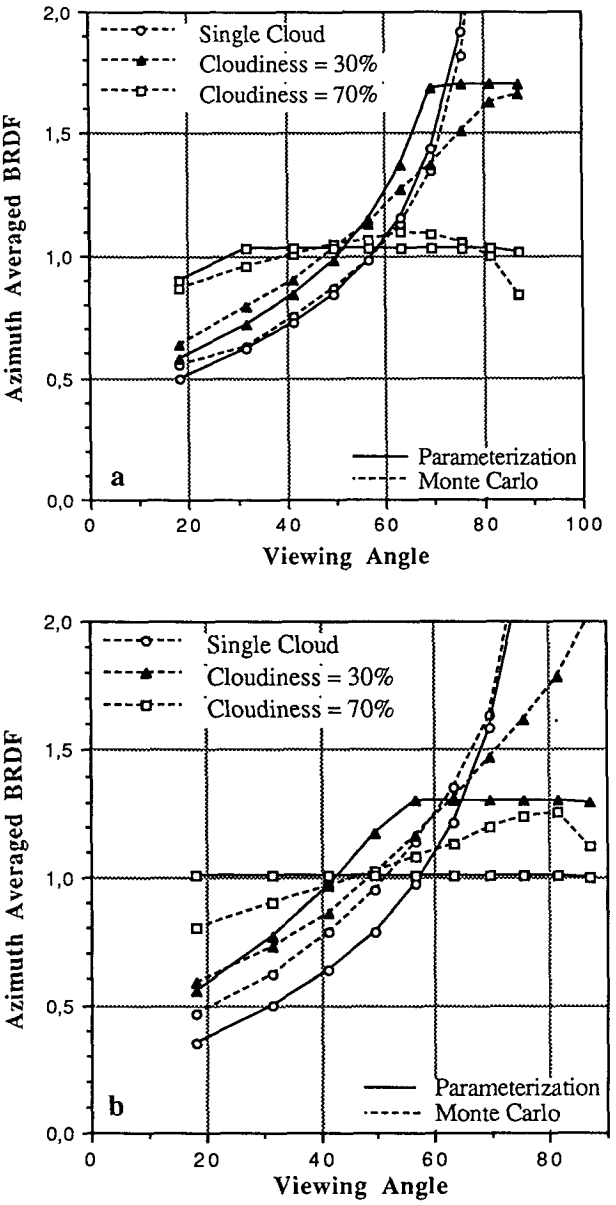

FIG. 10. Azimuth-averaged reflectance function for regular arrays of cylindrical *clouds* at varying cloudiness. The plain curve shows the parameterization results; the dashed curve depicts the MC simulations. Results are given for the single cloud limit case (circles) and a cloudiness of 30% (triangles) and 70% (squares). For (a) the aspect ratio is 1 and the solar zenith angle is 45°. For (b) the aspect ratio is 0.5 and the solar zenith angle is 60°. The cloud optical thickness is 50.

Overall, the mean accuracy of the parameterization, when compared to the MC computations, is better than 10%. It confirms the hypothesis that, when azimuth averaged, the reflectance function is dominated by side-viewing and intercloud shadowing effects. Clearly, the assumptions made to derive the parameterization do not hold for some solar/cloud geometries, however.

For large solar zenith angles, the phase function forward peak leads to a radiance maximum at large viewing zenith angle in the forward direction. This maximum is clearly present even on azimuth-averaged results. Our hypothesis of radiance isotropy from each face fails, therefore, in the case of large solar zenith angles. Similarly, as the cloudiness increases, the BRDF tends to the plane parallel case and the relative importance on the BRDF of cloud-side viewing decreases. Our parameterization then will not describe the most important phenomena that drive the phase function. Last, for small cloud optical thicknesses, the BRDF is dominated by phase function effects, and our parameterization does not describe the main processes leading to the BRDF. For other geometries, that is, solar zenith angle smaller than 60°, medium or small cloudiness, or medium or large optical thicknesses, one can expect accuracies as shown in Fig. 10.

The parameterization provides a simple way to obtain the zenithal distribution of radiance exiting a broken cloud field, which might be useful for cloud–radiation interaction studies. It should be pointed out, however, that the cloud description, as used in our MC computations, is very crude. The clouds, for instance, are approximated as being (i) internally homogeneous, (ii) of simple geometry, and (iii) in a regular array.

Although clouds are clearly not internally homogeneous (Stephens and Platt 1987), effects of inhomogeneity on the reflected radiance has yet to be fully studied. It is therefore not clear whether internal homogeneities have an effect on the directional reflectance of a cloud field. A fractal liquid water distribution (Davis et al. 1990; Gabriel et al., 1990) could be a fruitful approach for computing the radiative transfer within a cloud.

To represent broken clouds we used an array of cylinders rather than cubes because they seemed closer to the real world. Real broken cloud shapes, however, are far more complex than simple cylinders. Cubic and cylindric geometries lead to similar results when studying the cloud field reflectance. Our hypothesis that each cloud face scatters radiance isotropically explains the similar behavior of cubic and cylindric *clouds*. Extended to more complex shaped clouds, we find that the cloud aspect ratio is an important parameter but that the cloud surface complexity does not have to be fully described.

In our study, the cylinders are arranged in a regular array in order to simplify the programming. In the Davies (1984) MC study, the azimuth-averaged reflectance of a regular cloud array was compared to that of a cloud field with random intercloud distance. Results were quite similar, suggesting that the regular array approximation is not critical.

Because the cloud field description is rather crude in our MC simulations, there is no evidence that it describes quantitatively correct *real* cloud field reflectance. Monte Carlo results, as well as the parameterization based on its results, should therefore be used with caution. In general, Monte Carlo methods applied to cloud radiative transfer should be used to infer the sensitivity of various parameters rather than to give quantitative values.

7. Summary and conclusion

This paper reports on a theoretical Monte Carlo study of the bidirectional reflectance distribution functions (BRDFs) for plane parallel and broken clouds. While many BRDFs were investigated for a large number of cloud and sun geometries, only a selected number could be reported in this paper. We summarized the various effects that lead to cloud reflectance anisotropy. These effects are schematically illustrated in Fig. 11.

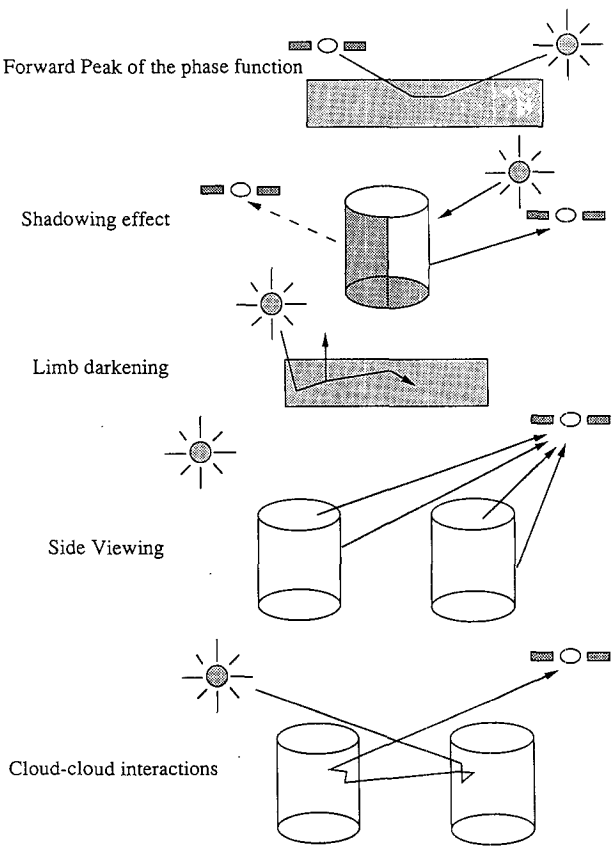

FIG. 11. Some of the processes leading to anisotropy of the radiation scattered by clouds. The forward peak of the phase function leads to higher fluxes in the direction away from the sun. The self-shadowing of a thick broken cloud leads to more radiation toward the sun. Limb darkening is due to an increased probability of extra scattering of photons moving close to the horizontal. Cloud-side flux gives, for broken clouds only, an increased flux toward the limb. Cloud–cloud interactions lead to complex processes such as intercloud shadowing of incoming and outgoing radiation.

For plane parallel clouds the two major effects are 1) limb darkening that reduces the BRDF at the limb viewing, down to 0.5 when the sun is at the zenith, and 2) a forward maximum, noticeable for solar zenith angles larger than 45°, due to the forward peak of the phase function. This effect leads to BRDFs up to 2.5 at the limb viewing in the direction away from the sun for a solar zenith angle of 60°. As the cloud optical thickness increases, the forward maximum gradually weakens as the limb darkening increases.

We show that side viewing of broken clouds greatly increases the radiance observed at large viewing zenith angles. For an isolated cloud, which is the limit case for low cloudiness, the BRDF displays a dependence close to $A + B \tan(\theta_v)$, where A and B depend on cloud geometry and optical thickness but not on zenith viewing angle, θ_v. This main zenithal dependance of the reflected flux can be modeled, considering that each cloud face is an isotropic emitter. For solar zenith angles different than 0°, other factors modify the BRDF: 1) the forward peak of the phase function creates a local maximum away from the sun, and 2) the varying illumination of the cloud side leads to a maximum toward the sun.

When studying an array of clouds the situation is more complex because, added to the effects already mentioned, cloud–cloud interactions occur, such as the mutual shadowing of incoming and outgoing radiation. These effects strongly depend on the relative distance between clouds as well as their mutual organization. For low cloudiness, the cloud field BRDF tends to the single cloud equivalent, except at the largest viewing zenith angles where mutual cloud shadowing reduces the BRDF. For increased cloudiness, the cloud field BRDF closes to the plane parallel equivalent, but with a brightening rather than a darkening toward the limb.

A parameterization is subsequently proposed for the azimuth-averaged cloud field reflectance based on the observation that, in the case of broken cloudiness, the reflectance function shape is primarily a result of cloud side viewing and intercloud shadowing. The few coefficients needed for the parameterization were fitted from a large set of Monte Carlo simulations with varying cloudiness, optical thickness, aspect ratios, and solar zenith angles. The resulting parameterization performs reasonably well when compared to Monte Carlo simulations. It could be used for cloud–radiation interaction modeling when an estimate of the zenithal distribution of radiation exiting the cloud field is needed.

Satellite estimates of cloud albedo are needed for radiation budget studies. Because the cloud field reflectance anisotropy is large and highly dependent on cloud geometry, physical models have to be developed to obtain cloud field BRDFs. The parameterization developed in the present study could be suitable for that purpose, but only for small solar zenith angles. For larger solar zenith angles, BRDFs become excessively azimuth dependent and our parameterization of azimuth-averaged functions does not apply. Anyhow, Monte Carlo simulations should be used in their present state to understand processes that modify cloud reflectance and albedo, rather than to quantify these processes. Although the Monte Carlo method has the potential of providing very accurate results, a better cloud field description is first needed. It seems from our limited simulations that the primary parameter is the cloud surface interception area and that the cloud shape is a secondary parameter. The liquid water distribution (droplet size and spatial distributions) within clouds, however, might be of crucial importance.

As long as Monte Carlo simulations are not validated against real cloud reflectance observations, the validity of such cloud approximations will not be demonstrated, and it would be dangerous to use these simulations rather than empirical BRDFs to correct cloud reflectance satellite observations. From his Monte Carlo simulation results, Davies (1984) shows that the BRDFs departure from one is usually minimal for a viewing angle of 60° and therefore recommends giving a larger weight to such observations when estimating radiation budgets from averaged satellite measurements. This procedure would reduce the estimate scatter around the sought value. One should note, however, that it could also introduce a bias in the estimate if the mean BRDF of the "real world" significantly departs from 1 at this particular angle. As the main concern is to obtain a nonbiased estimate of the upwelling flux, it is safer to average the observations for several viewing angle intervals and to give to each of these averages a weight equal to $\sin(\theta_v)\cos(\theta_v)$, which is the relative importance of each angle for the radiative budget.

Acknowledgments. This work was supported by NASA Grant NAG-1-889 and the California Space Institute. We would like to thank M. Herman and D. Crétel, from the Laboratoire d'Optique Atmosphérique, who worked on their model for a mutual validation. The editing help of B. Bloomfield and M. Petrie is greatly appreciated.

REFERENCES

Aida, M., 1977: Scattering of solar radiation as a function of cloud dimensions and orientation. *Quat. Spectrosc. Radiat. Transfer,* **17,** 303–310.

Bradley, S. G., 1981: The relation between cumulus albedo and extension coefficient and its application to remote sensing. *J. Atmos. Sci.,* **38,** 2243–2256.

Claußen, M., 1982: On the radiative interaction in three dimensional cloud fields. *Beitr. Phys. Atmos.,* **55,** 158–169.

Coakley, J. A., Jr., and T. Kobayashi, 1989: Broken cloud biases in albedo and surface insolation derived from satellite imagery data. *J. Climate,* 721–730.

Crétel, D., M. Herman, and D. Tanré, 1989: Fluxes and directional effects of broken clouds. *Proc. 1988 IRS Conference.* J. Lenoble and J.-F. Geleyn, Eds., A. Deepak, 95–98.

Davies, R., 1978: The effect of finite geometry on the tridimensional transfer of solar irradiance in clouds. *J. Atmos. Sci.,* **35,** 1712–1725.

——, 1984: Reflected solar radiances from broken cloud scenes and the interpretation of scanner measurement. *J. Geophys. Res.*, **89,** 1259–1266.

Davis, A., P. Gabriel, S. Lovejoy, D. Schertzer, and G. L. Austin, 1990: Discrete angle radiative transfer. 3. Numerical results and meteorological applications. *J. Geophys. Res. (Atmos.)*, **95,** 11 729–11 742.

Deirmendjian, D., 1969: *Electromagnetic Scattering on Sperical Polydispersions.* Elsevier, 290 pp.

Gabriel, P., S. Lovejoy, A. Davis, D. Schertzer, and G. L. Austin, 1990: Discrete angle radiative transfer. 2. Renormalization approach for homogeneous and fractal clouds. *J. Geophys. Res. (Atmos.)*, **95,** 11 717–11 728.

Jacobwitz, H., H. V. Soule, H. L. Kyle, F. B. House, and the *Nimbus-7*-ERB Experiment Team, 1984: The earth radiation budget experiment: An overview. *J. Geophys. Res.*, **89,** 5021–5038.

Kobayashi, T., 1988: Parameterization of reflectivity for broken cloud fields. *J. Atmos. Sci.*, **45,** 3034–3045.

——, 1989: Radiative properties of finite cloud fields over a reflecting surface. *J. Atmos. Sci.*, **46,** 2208–2214.

McKee, T. B., and S. K. Cox, 1974: Scattering of visible radiation by finite clouds. *J. Atmos. Sci.*, **31,** 1885–1892.

Minnis, P., and E. F. Harrison, 1984: Diurnal variability of regional cloud and clear-sky radiative parameters derived from GOES data. Part III: November 1978 radiative parameters. *J. Climate Appl. Meteor.*, **23,** 1032–1051.

Ruff, I., R. Koffler, S. Fritz, J. S. Winston, and P. K. Rao, 1968: Angular distribution of solar radiation reflected from clouds as determined from *TIROS-IV* radiometer measurements. *J. Atmos. Sci.*, **25,** 323–332.

Schmetz, J., 1984: On the parameterization of the radiative properties of broken clouds. *Tellus,* **36A,** 417–432.

Smith, G. L., R. N. Green, E. Raschke, L. M. Avis, J. T. Suttles, B. A. Wielicki, and R. Davies, 1986: Inversion methods for satellite studies of the earth's radiation budget: Development of algorithms for the ERBE mission. *Rev. Geophys.*, **24,** 407–421.

Stephens, G. L., 1978: Radiation profiles in extended water clouds. II: Parameterization schemes. *J. Atmos. Sci.*, **35,** 2123–2132.

——, and C. M. R. Platt, 1987: Aircraft observation of the radiative and microphysical properties of stratocumulus and cumulus cloud fields. *J. Climate Appl. Meteor.*, **26,** 1243–1269.

Taylor, V. R., and L. R. Stowe, 1984: Reflectance characteristics of uniform earth and cloud surfaces derived from *Nimbus-7* ERB. *J. Geophys. Res.*, **89,** 4987–4996.

Weinman, J. A., and Harshvardhan, 1982: Solar reflection from a regular array of horizontally finite clouds. *Appl. Optics,* **21,** 2940–2944.

Welch, R. M., and B. A. Wielicki, 1984: Stratocumulus cloud field reflected fluxes: The effect of cloud shape. *J. Atmos. Sci.*, **41,** 3085–3103.

——, and ——, 1985: A radiative parameterization of stratocumulus cloud fields. *J. Atmos. Sci.*, **42,** 2888–2897.

Wielicki, B. A., and R. A. Green, 1989: Cloud identification for ERBE radiative flux retrieval. *J. Appl. Meteor.*, **28,** 1133–1146.